

A Geometrically Exact Active Beam Theory for Multibody Dynamics Simulation

Dong Han, Wenbin Yu[‡], and Sitikantha Roy

Department of Mechanical and Aerospace Engineering, Utah State University, Logan, Utah
80322-4130, USA

E-mail: wenbin.yu@usu.edu

Abstract. A geometrically exact beam theory suitable for dynamic simulation of multibody systems involving active components is developed and implemented into a general-purpose multibody dynamics code. Taking advantage of the smallness of aspect ratio, we model the active beam as a generalized one-dimensional continuum with constitutive models obtained from a cross-sectional analysis. Various examples for both static and dynamic behavior of composite beams with embedded or attached piezoelectric layers or multibody systems with such components have been used to validate the theory and code. Good agreement is found with available results in the literature and commercial multiphysics simulation package. This work enables comprehensive analyses of multibody systems involving active beam components made of smart materials.

Submitted to: *Smart Materials and Structures*

Introduction

In recent years, there has been a strong interest in applying active materials to make military¹ and civil structures² “smart” so that they can sense and react to external stimuli and thus create the possibility of building self-monitorable and self-controllable systems to further improve the performance. Among many active materials (such as shape-memory alloys, magnetostrictives, piezoelectrics, electrostrictives, and etc.) for actuators and sensors, electromechanical materials such as piezoelectrics receive the most attention for two main reasons:³ (1) these materials directly relate electric signals to strains within the material and vice versa and thus can be used both as actuators and sensors, and (2) these materials have a wide range of high actuating and sensing frequencies which are suitable for real-time controlling and monitoring.

Although a tremendous amount of work on smart structures has been conducted in recent years,³⁻⁵ the analytical predictive capabilities for smart structures, particularly adaptive systems involving active components are still limited. Future adaptive systems could contain components of completely different natures such as rigid bodies, joints, springs, dampers, and

[‡] Corresponding author: +1-435-7978246 (tel.); +1-435-7972417 (fax)

flexible bodies made of passive or active materials. Authentic simulation of these systems calls for a genuine multibody approach.⁶

Gual et al.⁷ studied the damping performance of electromechanical materials by implementing active joint description in a hybrid multibody system. Rose et al.⁸ developed a multibody analysis by combining active modes from distributed piezoelectric actuators/sensors and natural modes to suppress undesirable vibrations of high-speed mechanisms. Ghiringhelli et al.⁹ incorporated smart beams made of active fiber composites in a multibody dynamics code MBDyn to develop an integrated tool for aeroelastic analysis of active rotors. Zhang et al.¹⁰ developed a method to analyze high-speed flexible linkage mechanisms with piezoelectric sensors and actuators. Straub and Charles¹¹ developed an aeroelastic analysis for a bearingless rotor with active trailing edge flaps using a finite-element based multibody code, CAMRAD II. Chopra and his co-workers developed a comprehensive finite element rotor analysis for active control surfaces¹² and for active blade tips.¹³ Cesnik and his co-workers studied the dynamic responses of active twist rotor¹⁴ based on the intrinsic formulation of moving beams derived by Hodges.¹⁵

In view of the existing studies, we adopt a different approach by developing a geometrically exact active beam element into a general-purpose, nonlinear flexible multibody code to enable a general-purpose multibody dynamics simulation for realistic systems with active components which can be sufficiently modeled as beams. Here we choose DYMORE as the platform for implementation due to its versatility in handling arbitrary topology of multibody systems, although it is obvious that the active beam element developed in this work can also be implemented into other multibody codes with no or little changes.

Three-dimensional Formulation

The elastodynamics of a structure is governed by the Hamilton's principle

$$\int_{t_1}^{t_2} [\delta(\mathcal{K} - \mathcal{U}) + \delta\overline{\mathcal{W}}] dt = \delta\overline{\mathcal{A}} \quad (1)$$

where t_1 and t_2 are arbitrary fixed times, \mathcal{K} and \mathcal{U} are the kinetic and internal energy, respectively, δ is the usual Lagrangean variation for a fixed time, $\delta\overline{\mathcal{W}}$ is the virtual work of applied loads and electric charges (if exist), and $\delta\overline{\mathcal{A}}$ is the virtual action at the ends of time interval and are usually discarded in the application of Hamilton's principle. The bars over variations are used to indicate that the virtual quantities need not be the variations of function or functionals. An active beam is a structure made of active materials, which implies that the internal energy will be characterized by the mechanical field and one or more other fields. For linear electromechanical materials such as piezoelectrics, which are the focus of the present work, the internal energy turns out to be the electric enthalpy

$$\mathcal{U} = \frac{1}{2} \int_{\mathcal{V}} (\Gamma^T : \mathbf{C}^E : \Gamma - 2\mathbf{E} \cdot \mathbf{e} : \Gamma - \mathbf{E}^T \cdot \boldsymbol{\epsilon}^\Gamma \cdot \mathbf{E}) d\mathcal{V} \quad (2)$$

where \mathbf{C}^E is the elastic tensor at constant electric field, Γ is the strain tensor, \mathbf{e} is the piezoelectric tensor, \mathbf{E} is the electric field vector, $\boldsymbol{\epsilon}^\Gamma$ is the dielectric tensor at constant strain

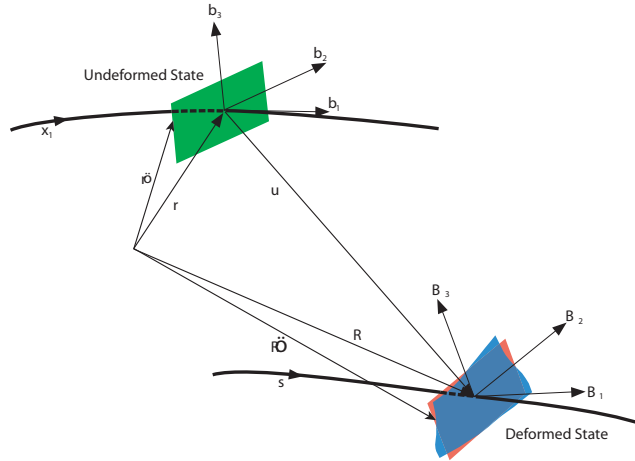


Figure 1. Schematic of beam deformation

field, and \mathcal{V} is the volume occupied by the structure.

As shown in Fig. 1, a beam can be represented by a reference line, described by its arc-length x_1 , and a typical reference cross section, described by local Cartesian coordinates x_α . (Here and throughout the paper, Greek indices assume values 2 and 3 while Latin indices assume 1, 2, and 3. Repeated indices are summed over their range except where explicitly indicated). At each point along the reference line, an orthonormal triad \mathbf{b}_i is introduced such that \mathbf{b}_i is tangent to x_i . Any point of the undeformed structure is then located by the position vector $\hat{\mathbf{r}}$ as

$$\hat{\mathbf{r}}(x_1, x_2, x_3) = \mathbf{r}(x_1) + x_\alpha \mathbf{b}_\alpha \quad (3)$$

where \mathbf{r} is the position vector of the points of the reference line, $\mathbf{r}' = \mathbf{b}_1$ and $()'$ means the derivative with respect to x_1 . It is noted that \mathbf{b}_i could be functions of x_1 due to existence of initial curvatures or twist, and they relate to the base vectors of the inertial frame \mathbf{I}_i using a direction cosine matrix C^{bI} such that $\mathbf{b}_i = C_{ij}^{bI} \mathbf{I}_j$.

We introduce another orthonormal triad \mathbf{B}_i to characterize the rotation of the cross section due to rigid body motion and elastic deformation of the reference line with \mathbf{B}_1 normal to the deformed reference cross section plane, and they relate to \mathbf{b}_i as

$$\mathbf{B}_i = \mathbf{C}^{Bb} \cdot \mathbf{b}_i = C_{ij}^{Bb} \mathbf{b}_j \quad (4)$$

where $\mathbf{C}^{Bb} = C_{ij}^{Bb} \mathbf{b}_i \mathbf{b}_j$ denotes the rotation tensor, and C_{ij}^{Bb} are the components of the corresponding direction cosine matrix. The deformed position, $\hat{\mathbf{R}}$, of the point which had $\hat{\mathbf{r}}$ in the undeformed state can be expressed as

$$\hat{\mathbf{R}}(x_1, x_2, x_3) = \mathbf{r}(x_1) + \mathbf{u}(x_1) + x_\alpha \mathbf{B}_\alpha + w_i(x_1, x_2, x_3) \mathbf{B}_i \quad (5)$$

where $\mathbf{u} = u_i \mathbf{b}_i$ is the displacement vector (including both rigid body motion and elastic deformation) of the reference line from the reference configuration and w_i are the warping functions.

Using the concept of decomposition of rotation tensor for small local rotation,¹⁶ we can express the Jaumann-Biot-Cauchy strains as

$$\Gamma_{ij} = \frac{1}{2}(F_{ij} + F_{ji}) - \delta_{ij} \quad (6)$$

where δ_{ij} is the Kronecker symbol, and F_{ij} the deformation gradient obtained using

$$F_{ij} = \mathbf{B}_i \cdot \mathbf{G}_k \mathbf{g}^k \cdot \mathbf{b}_j \quad (7)$$

with \mathbf{G}_k as the covariant base vectors of the deformed configuration and \mathbf{g}^k as the contravariant base vectors of the undeformed configuration.

A key step to construct a beam model is to express the three-dimensional (3D) strain field in terms of one-dimensional (1D) generalized strain measures, which are defined as¹⁷

$$\begin{aligned} \gamma_{11} \mathbf{b}_1 + 2\gamma_{12} \mathbf{b}_2 + 2\gamma_{13} \mathbf{b}_3 &= \mathbf{C}^{bB} \cdot (\mathbf{r}' + \mathbf{u}') - \mathbf{r}' \\ \kappa_i \mathbf{b}_i &= \mathbf{C}^{bB} \cdot \mathbf{K} - \mathbf{k} \end{aligned} \quad (8)$$

where \mathbf{K} is the curvature vector of the deformed reference line, \mathbf{k} is the curvature vector of the undeformed reference line, γ_{11} is the extensional strain, $2\gamma_{1\alpha}$ are transverse shear strains, κ_1 is the twist, and κ_α are the bending curvatures. When the two superscripts of the rotation tensor are switched, it means the transpose of the original tensor, *e.g.*, $\mathbf{C}^{bB} = (\mathbf{C}^{Bb})^T$, and the same rule applies to the corresponding rotation matrix.

A complete description of active beams requires not only the mechanical field but also the electric field, which is defined in terms of the electric potential, $\phi(x_i)$, as

$$\mathbf{E} = -\nabla \phi = -\frac{\partial \phi}{\partial x_i} \mathbf{g}^i \quad (9)$$

The electric enthalpy can be easily calculated by substituting Eqs. (6) and (9) into Eq. (2).

To calculate the kinetic energy, we can follow Hodges¹⁷ to obtain the absolute velocity of a generic point M in the structure by taking a time derivative of Eq. (5), such that

$$v = V + \tilde{\Omega}(\xi + w) + \dot{w} \quad (10)$$

where $(\dot{\quad})$ is the partial derivative with respect to time, V is the absolute velocity of a point in the deformed reference line, Ω is the inertial angular velocity of \mathbf{B}_i bases, and the notation $\tilde{(\quad)}$ forms an antisymmetric matrix from a vector according to $\tilde{(\quad)}_{ij} = -e_{ijk}(\quad)_k$ using the permutation symbol e_{ijk} . From the definitions of V and Ω , we have

$$V = C^{BI} \dot{u}_I \quad (11)$$

$$\tilde{\Omega} = -\dot{C}^{BI} C^{IB} \quad (12)$$

with $C^{BI} = C^{Bb} C^{bI}$. In Eq. (10), the symbols v, V, Ω, w denote column matrices containing the corresponding components in \mathbf{B}_i bases, and $\xi = [0 \ x_2 \ x_3]^T$. The kinetic energy of a beam can be obtained by

$$\mathcal{K} = \frac{1}{2} \int_{\mathcal{V}} \rho v^T v d\mathcal{V} = \mathcal{K}_{1D} + \mathcal{K}^* \quad (13)$$

where ρ is the mass density and

$$\mathcal{K}_{1D} = \frac{1}{2} \int_0^L (\mu V^T V + 2\Omega^T \widetilde{\mu \bar{\xi}} V + \Omega^T i \Omega) dx_1 \quad (14)$$

$$\mathcal{K}^* = \frac{1}{2} \int_{\mathcal{V}} \rho \left[(\widetilde{\Omega} w + \dot{w})^T (\widetilde{\Omega} w + \dot{w}) + 2(V + \widetilde{\Omega} \xi)^T (\widetilde{\Omega} w + \dot{w}) \right] d\mathcal{V} \quad (15)$$

where in Eq. (14), L is the length of the beam, and μ , $\mu \bar{\xi}$, and i are defined as mass per unit length, the first and second distributed mass moments of inertia respectively, which can be trivially obtained through simple integrals over the cross section.¹⁷

If no electric charges applied on the surfaces or inside the body, the virtual work of the active beam is completely due to applied loads and can be calculated as

$$\overline{\delta \mathcal{W}} = \int_0^L \left(\langle \mathbf{F} \cdot \delta \hat{\mathbf{R}} \sqrt{g} \rangle + \oint_{\partial \Omega} \mathbf{Q} \cdot \delta \hat{\mathbf{R}} ds \right) dx_1 + \langle \mathbf{Q} \cdot \delta \hat{\mathbf{R}} \rangle \Big|_{x_1=0}^{x_1=L} \quad (16)$$

where the angle brackets signify integration of the argument over the cross-sectional plane, g is the determinant of the metric tensor of undeformed geometry, $\partial \Omega$ denotes the lateral surface of the beam, $\mathbf{F} = F_i \mathbf{B}_i$ is the applied body force, $\mathbf{Q} = Q_i \mathbf{B}_i$ is the applied surface tractions. $\delta \hat{\mathbf{R}}$ is the Lagrangian variation of the displacement field, such that

$$\delta \hat{\mathbf{R}} = \overline{\delta q}_i \mathbf{B}_i + x_\alpha \delta \mathbf{B}_\alpha + \delta w_i \mathbf{B}_i + w_i \delta \mathbf{B}_i \quad (17)$$

where the virtual displacements and rotations are defined as

$$\overline{\delta q}_i = \delta \mathbf{u} \cdot \mathbf{B}_i \quad \delta \mathbf{B}_i = \overline{\delta \psi}_j \mathbf{B}_j \times \mathbf{B}_i \quad (18)$$

where $\overline{\delta q}_i$ and $\overline{\delta \psi}_i$ contain the components of the virtual displacements and rotations in the \mathbf{B}_i system, respectively. Since the warping functions are small, one may safely ignore products of the warping and virtual rotation in $\delta \hat{\mathbf{R}}$ and obtain the virtual work due to applied loads as

$$\overline{\delta \mathcal{W}} = \overline{\delta \mathcal{W}}_{1D} + \overline{\delta \mathcal{W}}^* \quad (19)$$

where

$$\overline{\delta \mathcal{W}}_{1D} = \int_0^L (f_i \overline{\delta q}_i + m_i \overline{\delta \psi}_i) dx_1 + \langle Q_i \rangle \overline{\delta q}_i \Big|_{x_1=0}^{x_1=L} + e_{i\alpha j} \langle x_\alpha Q_j \rangle \overline{\delta \psi}_i \Big|_{x_1=0}^{x_1=L} \quad (20)$$

$$\overline{\delta \mathcal{W}}^* = \int_0^L \left(\langle F_i \sqrt{g} \delta w_i \rangle + \oint Q_i \delta w_i ds \right) dx_1 + \langle Q_i \delta w_i \rangle \Big|_{x_1=0}^{x_1=L} \quad (21)$$

with the generalized forces f_i and moments m_i defined as

$$f_i = \langle F_i \sqrt{g} \rangle + \oint Q_i ds \quad m_i = e_{i\alpha j} \left(\langle x_\alpha F_j \sqrt{g} \rangle + \oint x_\alpha Q_j ds \right) \quad (22)$$

So far, we have transformed the original Hamilton's principle for the dynamics of electromechanically coupled problem for active beams into a four-field variational principle in terms of u_i (corresponding to $\overline{\delta q}_i$), C_{ij}^{Bb} (corresponding to $\overline{\delta \psi}_j$), w_i , and ϕ . If we attempt to

solve this problem directly, we will meet the same difficulty as solving any full 3D problem. The main complexity comes from the unknown 3D warping functions, w_i and 3D electric potential function, ϕ . The common practice in the literature is to assume w_i , *a priori*, in terms of 1D functions, u_i and C_{ij}^{Bb} , and ϕ in terms of applied electric potential to straightforwardly reduce the original 3D continuum model into a 1D beam model. However, for beams made with generally composite materials, the imposition of such *ad hoc* assumptions may introduce significant errors. The accuracy of the reduced beam model becomes worse when there exist multiple fields in the structure. Recently, the variational asymptotic method (VAM) of Berdichevsky¹⁸ is used to eliminate the warping functions through a two-dimensional (2D) cross-sectional analysis.¹⁹ The cross-sectional analysis of smart beams is an important subject by itself, which is out of the scope of the present work. Without repeating the entire analysis here, we will simply state the results which is sufficient for us to formulate the geometrically exact active beam theory. Ref. [19] showed that the original 3D variational statement can be approximated by the following 1D variational statement

$$\int_{t_1}^{t_2} [\delta(\mathcal{K}_{1D} - \mathcal{U}_{1D}) + \delta\overline{\mathcal{W}}_{1D}] dt = 0 \quad (23)$$

where \mathcal{U}_{1D} is the 1D internal energy which has the following symbolical form

$$\mathcal{U}_{1D} = \frac{1}{2} \int_0^L \left(\begin{Bmatrix} \gamma \\ \kappa \end{Bmatrix}^T \begin{bmatrix} A & B \\ B^T & D \end{bmatrix} \begin{Bmatrix} \gamma \\ \kappa \end{Bmatrix} - 2 \begin{Bmatrix} \gamma \\ \kappa \end{Bmatrix}^T \begin{Bmatrix} F^e \\ M^e \end{Bmatrix} \right) dx_1 \quad (24)$$

where $\gamma = [\gamma_{11} \ 2\gamma_{12} \ 2\gamma_{13}]^T$ and $\kappa = [\kappa_1 \ \kappa_2 \ \kappa_3]^T$, F^e and M^e are stress resultants due to applied load and electric field, and A, B, D are sub matrices of the stiffness matrix of the beam cross section. The details of calculating A, B, D, F^e , and M^e in terms of material properties, electric field, warping functions, and cross section geometry are also provided in Ref. [19].

Formulation of the Geometrically Exact Active Beam Theory

If one chooses to work with body attached frames, it is straightforward to follow Hodges¹⁷ to derive the geometrically exact theory for active beams with the only change coming from the bilinear terms in the 1D internal energy, Eq. (24). However, as pointed out by Bauchau and Kang²⁰ to develop general-purpose computer codes for dynamic simulation of multibody systems with arbitrary topology, it is more advantageous to choose a single inertial Cartesian coordinate system as the reference. Furthermore, to facilitate the dynamic simulation of multibody simulations, we need to develop a displacement-based formulation instead of the intrinsic formulation of Hodges¹⁷. Hence, we will instead develop a displacement-based, geometrically exact active beam theory in an inertial frame so that it can be easily implemented into an inertial frame based multibody dynamic simulation code, such as DYMORE. To achieve this, we need to express the 1D variational statement, Eq. (23), in terms of beam displacements and rotations, which are our fundamental variables. Note the

rotations are described by C^{Bb} , an orthonormal matrix, which implies that its nine elements are not independent, and it can be characterized by using three or four parameters such as Euler parameters, Rodrigues parameters, or Wiener-Milenkovic parameters. In this work, we use the Wiener-Milenkovic parameters, to be consistent with DYMORE.

The components of the curvature vector of undeformed beam reference line in \mathbf{b}_i can be obtained from

$$\tilde{k} = -(C^{bI})'C^{Ib} \quad (25)$$

and the components of the curvature vector of deformed beam reference line in \mathbf{B}_i can be obtained from

$$\tilde{K} = -(C^{BI})'C^{IB} \quad (26)$$

From Eqs. (8), (25), and (26), we can obtain the 1D generalized strains in terms of displacements and rotation matrix as

$$\gamma = C^{BI}(r'_I + u'_I) - e_1 \quad (27)$$

$$\tilde{\kappa} = \tilde{K} - \tilde{k} = C^{BI}(C^{IB})' + (C^{bI})'C^{Ib} \quad (28)$$

where r_I and u_I are the column matrices holding the corresponding three components of \mathbf{r} and \mathbf{u} in the inertial system, respectively, and $e_1 = [1 \ 0 \ 0]^T$.

To obtain the Euler-Lagrange equations for the variational statement in Eq. (23), we also need to obtain the variations of strain measures ($\delta\gamma$ and $\delta\kappa$) and variations of velocity measures (δV and $\delta\Omega$). The second definition in Eq. (18) implies

$$\widetilde{\delta\psi} = -\delta C^{Bb}C^{bB} \quad (29)$$

which further implies the following relations

$$\delta C^{Bb} = -\widetilde{\delta\psi}C^{Bb} \quad \delta C^{bB} = C^{bB}\widetilde{\delta\psi} \quad (30)$$

Carrying out a variation of Eq. (27), we obtain

$$\delta\gamma = \delta C^{Bb}C^{bI}(r'_I + u'_I) + C^{BI}\delta u'_I = -\widetilde{\delta\psi}C^{BI}(r'_I + u'_I) + C^{BI}\delta u'_I \quad (31)$$

Here we have taken advantage of the fact that $\delta C^{bI} = 0$ and $\delta r'_I = 0$ and the first relation in Eq. (30). It can be shown that the components of the virtual rotation in the inertial frame, $\widetilde{\delta\psi}_I$, are related with $\widetilde{\delta\psi}$ using the following formula

$$C^{BI}\widetilde{\delta\psi}_I = \widetilde{\delta\psi}C^{BI} \quad (32)$$

Using this relation, Eq. (31) can be simplified to be

$$\delta\gamma = C^{BI}[(\tilde{r}'_I + \tilde{u}'_I)\widetilde{\delta\psi}_I + \delta u'_I] \quad (33)$$

By simple analogy, we can obtain δV from Eq. (11) as

$$\delta V = C^{BI}(\tilde{u}_I\widetilde{\delta\psi}_I + \delta u_I) \quad (34)$$

From (28), we obtain

$$\delta\tilde{\kappa} = \delta\tilde{K} = \delta[-(C^{Bb}C^{bI})'C^{Ib}C^{bB}] = \delta[-(C^{Bb})'C^{bB} + C^{Bb}\tilde{k}_kC^{bB}] \quad (35)$$

Following a similar derivation in Hodges,¹⁷ we can derive a very simple formula for $\delta\kappa$ as

$$\delta\kappa = \overline{\delta\psi}' + \tilde{K}\overline{\delta\psi} \quad (36)$$

Using the fact that $\overline{\delta\psi} = C^{BI}\overline{\delta\psi}_I$ along with Eq. (26), we can further simplify the expression for $\delta\kappa$ as

$$\delta\kappa = C^{BI}\overline{\delta\psi}'_I + (C^{BI})'\overline{\delta\psi}_I + \tilde{K}C^{BI}\overline{\delta\psi}_I = C^{BI}\overline{\delta\psi}'_I \quad (37)$$

Similarly, we can obtain $\delta\Omega$ from Eq. (12) as

$$\delta\Omega = C^{BI}\overline{\delta\psi}_I \quad (38)$$

For the purpose to calculate the variation of 1D internal energy, Eq. (24), we introduce the following definition for sectional stress resultants

$$\begin{Bmatrix} F \\ M \end{Bmatrix} = \begin{bmatrix} A & B \\ B^T & D \end{bmatrix} \begin{Bmatrix} \gamma \\ \kappa \end{Bmatrix} - \begin{Bmatrix} F^e \\ M^e \end{Bmatrix} \quad (39)$$

with F, M as column matrices containing measure numbers of internal forces and moments in \mathbf{B}_i system and conjugate to γ and κ , respectively.

For the purpose to calculate the variation of 1D kinetic energy, Eq. (14), we introduce the following definition for sectional momenta

$$\begin{Bmatrix} P \\ H \end{Bmatrix} = \begin{bmatrix} \mu & -\widetilde{\mu\xi} \\ \widetilde{\mu\xi} & i \end{bmatrix} \begin{Bmatrix} V \\ \Omega \end{Bmatrix} \quad (40)$$

with P, H as column matrices containing measure numbers of linear and angular momenta in \mathbf{B}_i system and conjugate to V and Ω , respectively. Then the 1D variational statement, Eq. (23), can be rewritten as

$$\int_{t_1}^{t_2} \int_0^L (\delta V^T P + \delta\Omega^T H - \delta\gamma^T F - \delta\kappa^T M + \overline{\delta q}^T f + \overline{\delta\psi}^T m) dx_1 dt = 0 \quad (41)$$

where $\overline{\delta q}, f, \overline{\delta\psi}, m$ are column matrices containing the corresponding components in \mathbf{B}_i system. The two boundary terms in Eq. (20) are dropped here because they relate with the boundary conditions at the ends and will not affect the Euler-Lagrange equations corresponding to the variational statement in Eq. (23). The boundary conditions can be straightforwardly obtained if we know whether the displacements and rotations are free to vary or not.

Substituting Eqs. (33), (34), (37), and (38) along with $\overline{\delta q} = C^{BI}\delta u_I$ and $\overline{\delta\psi} = C^{BI}\overline{\delta\psi}_I$ in to Eq. (41), and performing the variation following the usual steps of calculus of variations, we obtain the following Euler-Lagrange equations

$$\begin{aligned} F'_I + f_I &= \dot{P}_I \\ M'_I + (\tilde{r}'_I + \tilde{u}'_I)F_I + m_I &= \dot{H}_I + \dot{\tilde{u}}_I P_I \end{aligned} \quad (42)$$

with the subscript I denoting the measure numbers in the inertial coordinate system, that is $F_I = C^{IB}F$, $P_I = C^{IB}P$, and etc.

The equations of motion in Eq. (42) along with the constitutive relations in Eqs. (39) and (40) and the kinematic relations in Eqs. (27), (28), (11), and (12) complete the formulation of the geometrically exact active beam theory. They are identically the same as those used for the beam element in DYMORE²¹ except the 1D constitutive model in Eq. (39). It is emphasized here that the internal forces and moments in the constitutive relation of active beam cross-section are composed of two parts. The first part corresponds to conventional composite beam cross-section stiffness and the second part corresponds to the piezoelectric constants (F^e , M^e) which reflects the fact that the beam is made of active materials. Although rigorous incorporation of the work done by applied loads through the warping functions into the cross-sectional analysis will also contribute to these terms, how important this contribution is will be investigated in the near future.

The constitutive relations in Eqs. (39) and (40) for general anisotropic and heterogeneous beams should be obtained outside DYMORE through a cross-sectional analysis. However, not all cross-sectional analysis is compatible with this geometrically exact beam element. The derivation in this section and the previous section demonstrate that the constitutive relations calculated by VABS (Variational Asymptotical Beam Sectional Analysis)¹⁹ are fully compatible with DYMORE because both the cross-sectional analysis and 1D beam analysis are derived systematically from the same framework.

In comparison to the geometrically exact beam theory in the \mathbf{B}_i system of Hodges,¹⁷ except the different 1D constitutive model in Eq. (39), the equations of motion and kinematic relations for γ and V are simpler than the corresponding equations of Hodges.¹⁷

Having laid out the theoretical foundations, we are ready to implement this geometrically exact beam theory as an active beam element into DYMORE. The above theoretical derivations have disclosed that the main changes come from F^e and M^e in Eq. (39), which means the active beam element can be developed by inheriting all the existing codes of DYMORE geometrically nonlinear beam element and create a new module for defining smart beam properties according to the new constitutive model in Eq. (39). When the electric field \mathbf{E} is applied as a time varying function, F^e and M^e also varies with time. And also in view of the rapid advance of material science and structural technology, the future active beams could also have time varying (or controlled) stiffness (A , B , D in Eq. (39) in addition to F^e , M^e) and mass properties (μ , $\mu\bar{\xi}$, i in (Eq. (40))). All these can be considered in the implementation of active beams. After this modification, DYMORE is capable to simulate the static or dynamic behavior of multibody systems involving active beam components with controlled stiffness and mass properties. Furthermore, the active beam element is also geometrically exact which means it can handle large elastic displacements and rotations.

Linear Statics of Active Composite Cantilever Beams

To facilitate the validation of this new element, we derive an analytical solution for linear statics of active composite cantilever beams through extending the solution of Hodges for

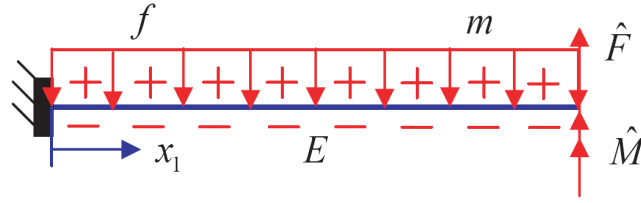


Figure 2. Configuration of a cantilevered active beam under tip and uniform distributed loads

end-loaded, prismatic, composite beams.¹⁷ For a cantilever under uniform distributed force f and moment m , tip force \hat{F} and moment \hat{M} as sketched in Fig. 2. The linear solution for u and θ can be expressed as

$$\begin{aligned}
 \theta &= (x_1 S^T + c_1 T \tilde{e}_1) \hat{F} + x_1 T (\hat{M} + M^e) + x_1 S^T F^e \\
 &\quad + (c_1 S^T + c_2 T \tilde{e}_1) f + c_1 T m \\
 u &= (x_1 R + c_1 S \tilde{e}_1 - \frac{1}{2} x_1^2 \tilde{e}_1 S^T - c_3 \tilde{e}_1 T \tilde{e}_1) \hat{F} \\
 &\quad + (x_1 S - \frac{1}{2} x_1^2 \tilde{e}_1 T) (\hat{M} + M^e) + (x_1 R - \frac{1}{2} x_1^2 \tilde{e}_1 S^T) F^e \\
 &\quad + \left[c_1 R + c_2 S \tilde{e}_1 - c_3 \tilde{e}_1 S^T - \frac{x_1^2}{24} (6L^2 - 4x_1 L + x_1^2) \tilde{e}_1 T \tilde{e}_1 \right] f \\
 &\quad + (c_1 S - c_3 \tilde{e}_1 T) m
 \end{aligned} \tag{43}$$

with

$$\begin{aligned}
 c_1 &= x_1 L - \frac{1}{2} x_1^2 \\
 c_2 &= \frac{x_1}{6} (x_1^2 - 3x_1 L + 3L^2) \quad \text{and} \quad \begin{bmatrix} R & S \\ S^T & T \end{bmatrix} = \begin{bmatrix} A & B \\ B^T & D \end{bmatrix}^{-1} \\
 c_3 &= \frac{x_1^2}{6} (3L - x_1)
 \end{aligned}$$

and u is a column matrix containing three displacements and θ is a column matrix containing three rotations. This closed-form solution can be used to evaluate the static behavior of cantilevered active beams with *full coupling* under uniform distributed loads and tip loads. This solution can also be generalized to other boundary conditions and load conditions. Such a solution will greatly facilitate the tailoring of active beams using both passive and active materials to maximize the performance. From the Eq. (43), we can observe that the tip moment \hat{M} and the actuation moment M^e can be combined (see the underlined terms) for both displacements and rotations. So we can conclude that if the uniformly distributed electric field on the cantilevered active beam has only moment effect, we can treat the piezoelectric moments equally as externally applied tip moments for evaluating the displacements and rotations. Later, we will verify whether this conclusion can be extended to the dynamic analysis of active beams.

Table 1. Cross-sectional constants for an active composite box beam

Stiffness	UM/VABS ²²
A_{11} (N)	9.951×10^5
A_{22} (N)	5.001×10^5
A_{33} (N)	3.839×10^5
D_{11} (Nm ²)	1.767×10^2
D_{22} (Nm ²)	1.014×10^2
D_{33} (Nm ²)	9.741×10^1
B_{31} (Nm)	-2.261×10^3
D_{13} (Nm ²)	1.500
$F_3^{(e)}$ (N)	-21.42
$M_1^{(e)}$ (Nm)	2.323

Numerical Examples

Several examples including active composite box beams, active laminated beams, and a simple multibody system are used to demonstrate the capability of the geometrically exact active beam theory as implemented in DYMORE to predict the static and dynamic behavior of active beams and multibody systems involving such components.

A composite box beam

To investigate the static and dynamic characteristics of active beams using present active beam theory, we first need to obtain the 1D constitutive model, Eq. (39). There are only a few existing results in the literature. Here we use an active composite beam corresponding to the s011-BB2t example studied by Palacios²² using UM/VABS²³. The cross-sectional properties excerpted from Ref. [22] are listed in Table 1, the piezoelectric constants (actuation force and torque) are generated due to application of a constant electric field.

The composite beam is cantilevered at the root with a span of 0.5 m. When we only apply the electric field, the static deformation of the beam can be easily computed using the linear solution in Eq. (43) and the geometrically exact active beam theory implemented in DYMORE. The beam is uniformly discretized by 20 second-order elements. The tip displacements and rotations calculated using these two approaches are listed in Table 2 along with those of Ref. [22], which is calculated using a linear beam model. It can be easily observed that DYMORE results are in good agreement with the linear solution and Ref. [22], which means that geometrical nonlinearity effects are not significant for this case.

If the electric field does not exist and only a 100 N force is applied at the tip of the active composite box beam along the x_3 direction, the tip displacements obtained using these approaches are listed in Table 3. These results show that the beam under this load have a strong geometrical nonlinearity which is demonstrated by the not negligible differences

Table 2. Tip displacements with piezoelectric actuation

Displacement	Ref. [22]	Linear	DYMORE
u_1 (mm)	0.000	0.000	0.000
u_2 (mm)	-0.025	-0.026	-0.026
u_3 (mm)	0.012	0.012	0.012
θ_1 (deg)	0.386	0.385	0.385
θ_2 (deg)	0.000	0.000	0.000
θ_3 (deg)	-0.006	-0.006	-0.006

Table 3. Tip displacements with 100 N tip load

Displacement	Ref. [22]	Linear	DYMORE
u_1 (mm)	0.00	0.00	-2.01
u_2 (mm)	0.00	-0.01	-0.01
u_3 (mm)	41.20	41.23	40.95
θ_1 (deg)	0.10	0.10	0.10
θ_2 (deg)	-7.06	-7.06	-7.03
θ_3 (deg)	0.00	0.00	0.00

between DYMORE results and the linear ones, particularly the significant axial deformation (u_1) obtained by the geometrically exact active beam element implemented in DYMORE.

When both the electric field and tip load are applied, the displacements obtained by the linear solution will be a simple addition of the results in Table 2 and Table 3 due to the superposition principle of linear theory. However, the results obtain using DYMORE results are slightly different from the those obtained by simply superposition because this rule does not apply to nonlinear theories.

This example shows that the geometrically exact beam element implemented in DYMORE produces expected results providing the cross-sectional properties of active beams are given in the form of Eq. (39).

A three-layer composite beam

A cantilevered three-layer composite beam of rectangular section is studied intensively in literature.^{24–26} This active beam is built up by an aluminum substrate, a piezoelectric layer and an adhesive layer. Constant electric voltage 12.49 kV is applied on the surface of the piezoelectric layer. Table 4 shows the geometry and material data of the active beam.

To analyze this beam using the present approach, we need to obtain the cross-sectional properties first and then use DYMORE to calculate the 1D global behavior. The cross-sectional analysis of act beams is an important subject by itself and has been investigated in Ref. 19. Here, we use VABS, a cross-sectional analysis code of active beams resulting

Table 4. Geometry and material properties of the three-layer active beam

Properties	Aluminium	Adhesive	Piezoelectric
E_{11} (GPa)	68.9	6.9	68.9
$E_{22} = E_{33}$ (GPa)	68.9	6.9	48.3
ν_{13}	0.25	0.4	0.25
$G_{12} = G_{13} = G_{23}$ (GPa)	27.6	2.46	20.7
e_{31} ($\frac{C}{m^2}$)	0	0	-6.54
e_{32} ($\frac{C}{m^2}$)	0	0	-4.14
e_{33} ($\frac{C}{m^2}$)	0	0	11.58
$\varepsilon_{11} = \varepsilon_{22} = \varepsilon_{33}$ ($\frac{C}{Vm}$)	10.18×10^{-11}	11.53×10^{-9}	11.53×10^{-9}
Thickness (mm)	15.24	0.254	1.524
Width (mm)	25.4	25.4	25.4
Density(kg/m ³)	2769	1662	7600

from Ref. 19. For the purpose of validation, we also calculate the cross-sectional properties using UM/VABS, a cross-sectional analysis code of active beams resulting from Ref. 23. We mesh this cross section with 100 8-noded quadrilateral elements (ten elements along the width, six elements along the thickness of the aluminum layer, two elements along the thickness of the adhesive layer and the piezoelectric layer). The non-zero elements of the cross-sectional stiffness matrix and piezoelectric resultants computed by these two computer codes are listed in Table 5. It can be observed that these two sets of results are very close to each other. However, it is noted that UM/VABS results are obtained using a one-way coupled approach because the generalized Timoshenko model, Eq. (39) are not available from the fully coupled approach of the current version of the code, while VABS results are obtained from a fully coupled approach. Both codes also obtain the same sectional mass properties as

$$\mu = 1.37678\text{kg/m} \quad i_2 = 3.98105 \times 10^{-5}\text{kg} \cdot \text{m} \quad i_3 = 7.40205 \times 10^{-5}\text{kg} \cdot \text{m}$$

along with the center of mass located at $x_2 = 0$ mm, $x_3 = 1.0167$ mm. Here μ denotes mass per unit span and i_α is the cross-sectional rotary inertia term associated with bending around x_α .

Having the cross-sectional properties, we can use DYMORE to compute the 1D global behavior including both static deformations and natural frequencies. Here we used 30 second-order active elements to mesh the beam axis. Table 6 shows the tip displacements of the active composite beam normalized by the thickness of the beam (H) predicted by different approaches, where ‘‘U/V+D’’ denotes DYMORE results with the cross-sectional constants computed by UM/VABS, ‘‘V+D’’ denotes DYMORE results with the cross-sectional constants computed using VABS, ‘‘RR’’ denotes the results of Robbins and Reddy²⁴ ‘‘SH’’ denotes the results of Saravanos and Heyliger²⁵ and ‘‘linear’’ denotes the results calculated using Eq. (43). From Table 6, we can see that DYMORE results are in close agreement with those results of Robbins and Reddy²⁴ and Saravanos and Heyliger²⁵ while the linear prediction of axial displacement is slightly more rigid, although it is small in comparison to the deflection.

Table 5. Cross-sectional constants for the three-layer active beam

UM/VABS		VABS	
Parameter	Value	Parameter	Value
$A_{11}(\text{N})$	2.938370×10^7	$A_{11}(\text{N})$	2.938370×10^7
$A_{22}(\text{N})$	9.567624×10^6	$A_{22}(\text{N})$	9.567624×10^6
$A_{33}(\text{N})$	9.420420×10^6	$A_{33}(\text{N})$	9.421221×10^6
$B_{12}(\text{Nm})$	-2.735132×10^3	$B_{12}(\text{Nm})$	-2.735121×10^3
$B_{21}(\text{Nm})$	3.379332×10^3	$B_{21}(\text{Nm})$	3.379342×10^3
$D_{11}(\text{Nm}^2)$	6.273437×10^2	$D_{11}(\text{Nm}^2)$	6.273438×10^2
$D_{22}(\text{Nm}^2)$	7.000224×10^2	$D_{22}(\text{Nm}^2)$	7.000603×10^2
$D_{33}(\text{Nm}^2)$	1.579765×10^3	$D_{33}(\text{Nm}^2)$	1.579765×10^3
$F_1^e(\text{N})$	2.670391×10^3	$F_1^e(\text{N})$	2.663376×10^3
$M_2^e(\text{Nm})$	2.069045×10^1	$M_2^e(\text{Nm})$	2.063140×10^1

Table 6. Tip displacements of the three-layer active beam

Displacement	RR	SH	Linear	U/V+D	V+D
$u_1(\times 10^4)/H$	8.024	8.028	8.366	8.078	8.057
$u_3(\times 10^2)/H$	-2.039	-2.040	-2.036	-2.042	-2.036

Table 7. Natural frequencies of the three-layer active beam

Frequency	RR	SH	KI	U/V+D	V+D
1 (F)	537.8	538.1	538.60	537.61	537.62
2 (F)	3196	3199	3211.00	3183.2	3183.3
3 (A)	7577	7580	7580.3	7574.9	7574.9
4 (F)	8340	8350	8394.86	8261.0	8261.3
5 (F)	15016	15039	15139.53	14766.5	14767.0

Table 7 lists the first five natural frequencies (including the first four flap (F) modes and the first axial (A) mode) predicted by different approaches including Robbins and Reddy,²⁴ Saravanos and Heyliger,²⁵ and Krommer and Irschik (denoted using ‘‘KI’’)²⁶ The case we studied is so-called close-circuit situation with both surfaces having prescribed electric potentials. From Table 7, we can conclude that DYMORE results agree with other approaches very well. The general trend is that higher modes have more differences among different approaches than lower modes.

It is worthy to point out that the computational effort of the present approach is equivalent to that of a 1D Timoshenko beam analysis while Refs. 24 and 25 use a layerwise approach and require more computational effort.

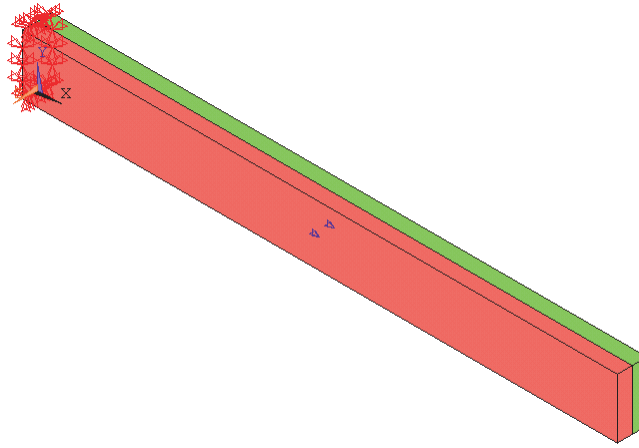


Figure 3. The two-layer beam modeled using ANSYS

A two-layer composite beam

The ultimate validation of any beam theory will be the original 3D analysis. For this purpose, we will use ANSYS, a commercial finite element package having multiphysics simulation capability, to further validate the present beam theory and the active beam element implemented in DYMORE. The example is a two-layer cantilevered beam built up by aluminium and PZT4 with the material properties of aluminum already given in Table 4. The material properties of PZT4 are

$$\begin{aligned}
 E_{11} = E_{22} &= 81.3 \text{ GPa} & E_{33} &= 64.5 \text{ GPa} & \nu_{12} &= 0.329 & \nu_{23} &= 0.432 \\
 G_{12} &= 30.6 \text{ GPa} & G_{13} = G_{23} &= 25.6 \text{ GPa} & e_{31} = e_{32} &= -5.2 \text{ (C/m}^2\text{)} \\
 e_{24} = e_{15} &= 12.7 \text{ (C/m}^2\text{)} & e_{33} &= 15.08 \text{ (C/m}^2\text{)} & \varepsilon_{33} &= 5.874 \times 10^{-9} \text{ C/Vm} \\
 \varepsilon_{11} = \varepsilon_{22} &= 6.761 \times 10^{-9} \text{ C/Vm} & \text{Density} &= 7500 \text{ kg/m}^3
 \end{aligned}$$

The width is 20 mm and the thickness of each layer is 5 mm. The length of the beam is 200 mm. Uniform electric field with 10 kV is applied on the surface of the PZT4 layer, and the voltage of the interface is 0 V; see Fig. 3. We mesh this cross section with 80 8-noded quadrilateral elements (twenty elements along the width, two elements along the thickness of each layer). The beam is uniformly meshed by 30 second-order elements. In ANSYS, 5000 SOLID5 element are used to calculate the static and dynamic behavior. In ANSYS, we constrained all the degrees of freedom of the four edges at the root surface to mimic a cantilever condition. The non-zero elements of cross-sectional stiffness matrix and piezoelectric constants computed by VABS and UM/VABS are listed in Table 8. Both codes obtain the same sectional mass properties as

$$\mu = 1.0269 \text{ kg/m} \quad i_2 = 8.5575 \times 10^{-6} \text{ kg} \cdot \text{m} \quad i_3 = 3.4230 \times 10^{-5} \text{ kg} \cdot \text{m}$$

along with the center of mass located at $x_2 = 0 \text{ mm}$, $x_3 = 1.1518 \text{ mm}$.

Table 8. Cross-sectional constants of the two-layer active beam

UM/VABS		VABS	
Parameter	Value	Parameter	Value
$A_{11}(\text{N})$	1.502536×10^7	$A_{11}(\text{N})$	1.502594×10^7
$A_{22}(\text{N})$	4.845536×10^6	$A_{22}(\text{N})$	4.845361×10^7
$A_{33}(\text{N})$	4.208792×10^6	$A_{33}(\text{N})$	4.198040×10^7
$B_{12}(\text{Nm})$	3.098881×10^3	$B_{12}(\text{Nm})$	3.062168×10^3
$B_{21}(\text{Nm})$	-4.203390×10^2	$B_{21}(\text{Nm})$	-4.248526×10^2
$D_{11}(\text{Nm}^2)$	1.301759×10^2	$D_{11}(\text{Nm}^2)$	1.301767×10^2
$D_{22}(\text{Nm}^2)$	1.252000×10^2	$D_{22}(\text{Nm}^2)$	1.277672×10^2
$D_{33}(\text{Nm}^2)$	5.007985×10^2	$D_{33}(\text{Nm}^2)$	5.008097×10^2
$F_1^e(\text{N})$	-2.022160×10^3	$F_1^e(\text{N})$	-2.024539×10^3
$M_2^e(\text{Nm})$	-4.995317	$M_2^e(\text{Nm})$	-4.843369

Table 9. Tip displacements of the two-layer active beam

Displacement	ANSYS	Linear	Error	U/V+D	Error	V+D	Error
$u_1(\text{mm})$	-0.0271	-0.0254	6.27%	-0.0272	0.37%	-0.0271	0.00%
$u_3(\text{mm})$	0.7157	0.7321	2.29%	0.7350	2.70%	0.6969	-2.63%

Table 9 shows the static beam tip displacements under the electric field. The relative error is calculated as $(\text{DYMORE}-\text{ANSYS})/|\text{ANSYS}|$. From Table 9, the DYMORE results have excellent agreement with the 3D nonlinear analysis with the maximum relative error less than 3%. It is noted that the linear prediction of the axial displacement is not so accurate because it is a linear theory.

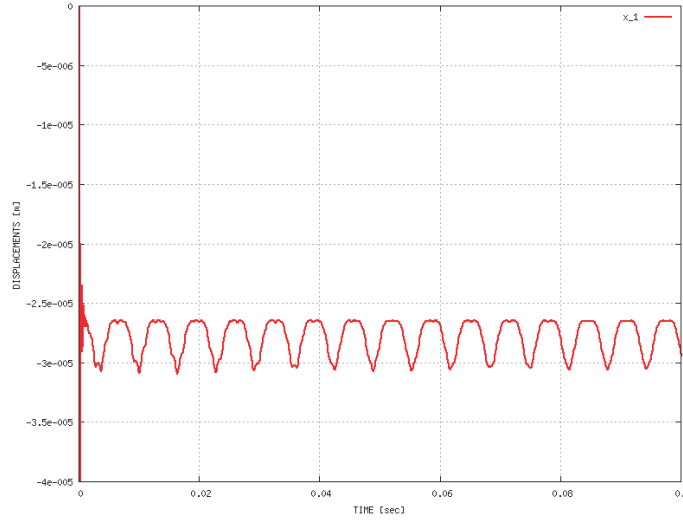
Table 10 shows the first ten natural frequencies computed by DYMORE and ANSYS, including the first four flap modes (F), the first two lag modes (L), the first three torsion modes (T) and the first axial mode (A). One can observe that the present theory, implemented using 1D active beam element in DYMORE, can accurately reproduce the natural frequencies calculated by the original 3D model up to the 10th mode with a maximum relative error less than 4%.

To show that the present theory implemented in DYMORE can also be used to investigate the dynamic behavior of active beams, we consider the electric field with the above voltage suddenly applied on the PZT4 layer at time $t = 0$ sec. We want to know how the structure behaves after the application of electric field till $t = 0.1$ sec. The transient dynamic responses of axial displacement u_1 and flap displacement u_3 at the tip are plotted in Figs. 4 and 5, respectively. From these figures we can observe that the dynamic responses of beam tip approximately move harmonically about the static equilibrium position.

We have concluded from Eq. (43) that actuation moment due to electricity is equivalent

Table 10. Natural frequencies of the two-layer active beam

Frequency	ANSYS	U/V+D	Error	V+D	Error
1 (F)	151.06	153.77	1.79%	155.35	2.84%
2 (L)	296.61	306.47	3.32%	306.48	3.33%
3 (F)	939.92	951.31	1.21%	960.86	2.23%
4 (L)	1791.8	1833.09	2.30%	1833.05	2.30%
5 (T)	2241.4	2218.17	-1.04%	2218.21	-1.03%
6 (F)	2598.1	2611.58	0.52%	2636.87	1.49%
7 (A)	4605.2	4775.35	3.69%	4776.73	3.72%
8 (T)	4750.8	4813.42	1.32%	4813.43	1.32%
9 (F)	5003.3	4987.69	-0.31%	5032.34	0.58%
10 (T)	6735.6	6659.22	-1.13%	6659.23	-1.13%

**Figure 4.** Time history of u_1 at the tip

to mechanical moments applied at the tip. We want to verify whether this conclusion is also applicable to dynamic responses. Imagining this two-layer beam has a special electric field so that the piezoelectric constants $F_1^e = 0$, we can compute the dynamic responses of the tip deflection due to piezoelectric constants M_2^e . We can also compute the dynamic responses of the tip deflection due to a tip moment $\hat{M} = M_2^e$. These two sets of results due to different load mechanisms are plotted in Fig. 6, which are identically to each other.

To show the versatility of the present theory and the DYMORE active beam element, we will carry out the dynamic simulation of a simple adaptive multibody system involving the two-layer active beam. This adaptive multibody system is formed with the active beam connecting via a revolute joint to a ground support which is rotating a speed of 62.8 rad/sec. The revolute joint is free to rotate around x_2 axis. The active beam is subjected to a time-varying electric field as shown in Fig. 7. This simple multibody system can be actually

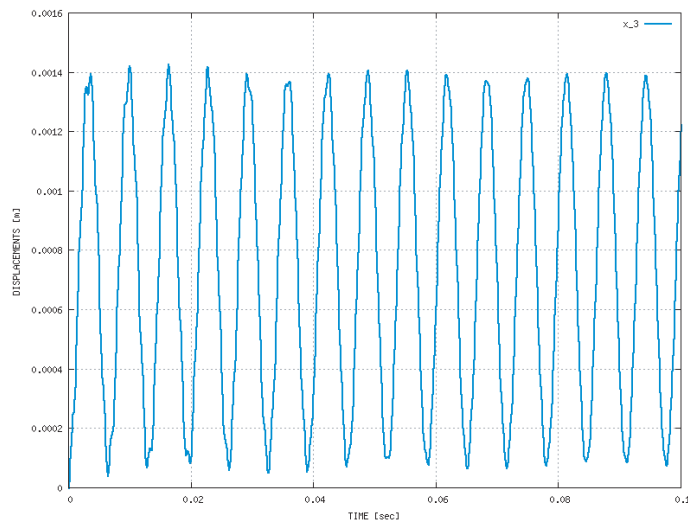


Figure 5. Time history of u_3 at the tip

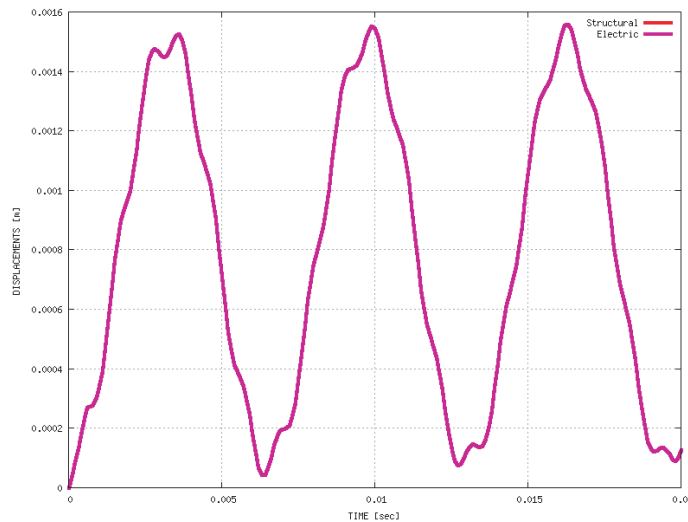


Figure 6. Comparison of u_3 due to different loading mechanisms

considered as a simplified model of an active helicopter rotor blade connecting to the hub with a flap hinge. The time histories of tip displacements in axial and flap directions are shown in Figs. 8 and 9, respectively. The responses of the displacements exhibit two distinguish frequencies, one is a high frequency motion representing the elastic deformation and the other is a low frequency motion representing the rigid rotation of the ground support.

Conclusions

A geometrically exact active beam theory suitable for multibody dynamics simulation has been developed for slender structures made of smart materials and has been implemented in DYMORE, a general-purpose multibody dynamics code. The resulting computational tool is capable of dynamic simulation of adaptive multibody systems involving smart beam

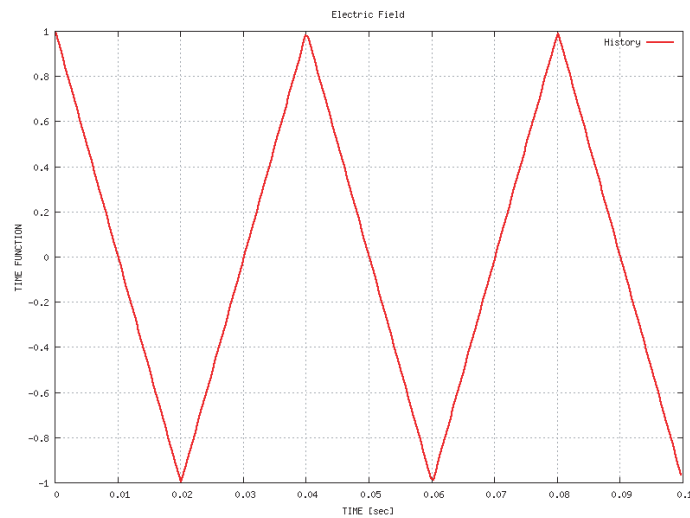


Figure 7. Time function of the electric field

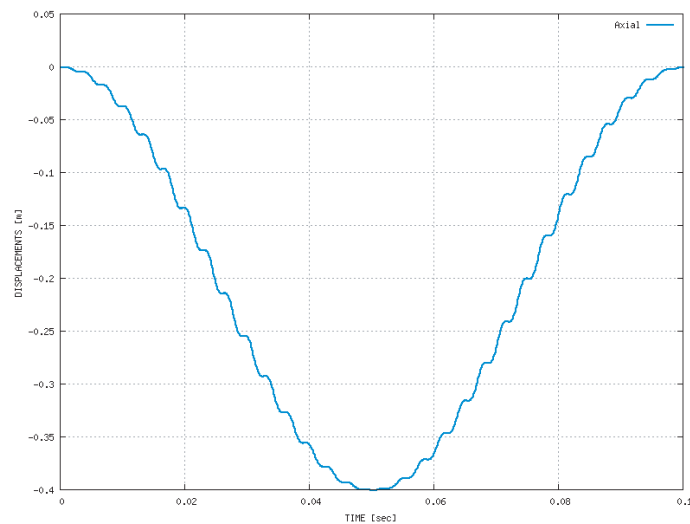


Figure 8. Time histories of u_1 at the beam tip of the simple multibody system

components which could have actively changing mass, stiffness and piezoelectric constants. A compact close-formed solution has been obtained for linear statics of active composite beam under tip and uniform distributed loads by specializing this new theory. Various examples including static, free vibration, and transient dynamic analysis of several typical composite beams and a simple multibody system have been used to demonstrate the application and predictability of the theory and the code. Excellent agreement has been found between the present theory and available results in the literature and commercial multiphysics software - ANSYS.

In addition to the development of a new tool for efficient high-fidelity design and analysis of multibody systems involving active beam components, this paper also clearly proves that the geometrically exact beam model constructed using the variational asymptotic method (represented by the VABS software) is fully compatible with the geometrically nonlinear beam

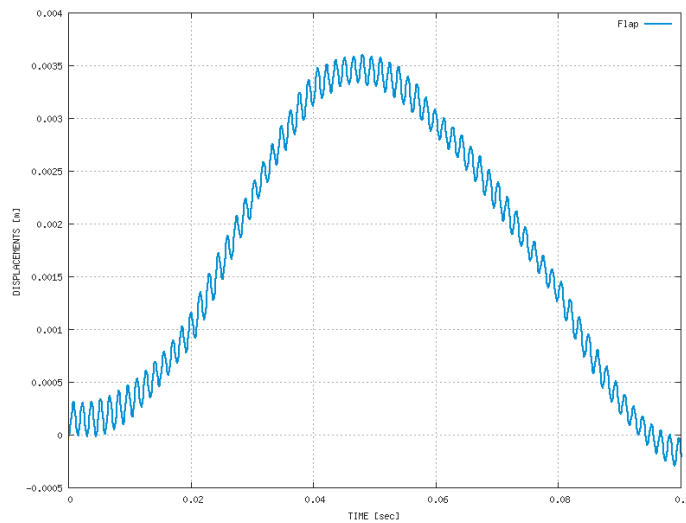


Figure 9. Time histories of u_3 at the beam tip of the simple multibody system

element used in DYMORE.

Acknowledgements

This work is partially supported by the Army Research Office under grant 49652-EG-II with Dr. Bruce LaMattina as the technical monitor, by the Georgia Tech Vertical Lift Research Center of Excellence, and the Space Dynamics Laboratory under Shunk Works Grant and Enabling Technologies Grant. The views and conclusions contained herein are those of the authors and should not be interpreted as necessarily representing the official policies or endorsement, either expressed or implied, of the funding agencies. The authors also want to thank Drs. Cesnik and Palacios at University of Michigan for the use of UM/VABS and technical discussions with Drs. Hodges and Bauchau at Georgia Tech.

- [1] Garg, D. P., Zikry, M. A., and Anderson, G. L., "Current and potential future research activities in adaptive structures: an ARO perspective," *Smart Materials and Structures*, Vol. 10, No. 4, 2001, pp. 610–623.
- [2] Chong, K. P., Carino, N. J., and Washer, G., "Health monitoring of civil infrastructures," *Smart Materials and Structures*, Vol. 12, 2003, pp. 483–493.
- [3] Chopra, I., "Review of state of art of smart structures and integrated systems," *AIAA Journal*, Vol. 40, No. 11, 2002, pp. 2145 – 2187.
- [4] Loewy, R. G., "Recent developments in smart structures with aeronautical applications," *Smart Materials and Structures*, Vol. 6, No. 5, October 1997, pp. R11–R42.
- [5] Giurgiutiu, V., "Review of smart materials actuation solutions for aeroelastic and vibration Control," *Journal of Intelligent Material Systems and Structures*, Vol. 11, 2000, pp. 525 – 544.
- [6] Huston, R., "Multibody Dynamics-Modeling and Analysis Method," *Applied Mechanics Reviews*, Vol. 44, No. 3, 1991, pp. 109 – 117.
- [7] Gaul, L., Lenz, J., and Sachau, D., "Active Damping of Space Structures by Contact Pressure Control in Joints," *Mechanics of Structures and Machines*, Vol. 26, No. 1, 1998, pp. 81–100.
- [8] Rose, M., Keimer, R., Breitbach, E. J., and Campanile, L. F., "Parallel Robots with Adaptronic

- Components,” *Journal of Intelligent Material Systems and Structures*, Vol. 15, No. 9-10, 2004, pp. 763 – 769.
- [9] Ghiringhelli, G. L., Masarati, P., and Mantegazza, P., “Analysis of an Actively Twisted Rotor by Multibody Global Modeling,” *Composite Structures*, Vol. 52, 2001, pp. 113–122.
- [10] Zhang, X., Shao, C., Shen, Y., and Erdman, A., “Complex Mode Dynamic Analysis of Flexible Mechanism Systems with Piezoelectric Sensors and Actuators,” *Multibody System Dynamics*, Vol. 8, 2002, pp. 51–70.
- [11] Straub, F. K. and Charles, B. D., “Aeroelastic analysis of rotors with trailing edge flaps using comprehensive codes,” *Journal of the American Helicopter Society*, Vol. 46, No. 3, 2001, pp. 192–199.
- [12] Koratkar, N. A. and Chopra, I., “Analysis and testing of Mach-scaled rotor with trailing-edge flaps,” *AIAA Journal*, Vol. 38, No. 7, 2000, pp. 1113 – 1124.
- [13] Bernhard, A. P. F. and Chopra, I., “Analysis of a bending-torsion coupled actuator for a smart rotor with active blade tips,” *Smart Materials and Structures*, Vol. 10, 2001, pp. 35–52.
- [14] Cesnik, C. E. S., Shin, S.-J., and Wilbur, M. L., “Dynamic Response of Active Twist Rotor Blades,” *Smart Materials and Structures*, Vol. 10, No. 1, February 2001, pp. 62–76.
- [15] Hodges, D. H., “A mixed variational formulation based on exact intrinsic equations for dynamics of moving beams,” *Int. J. Solids Structures*, , No. 11, 1990, pp. 1253–1273.
- [16] Danielson, D. A. and Hodges, D. H., “Nonlinear Beam Kinematics by Decomposition of the Rotation Tensor,” *Journal of Applied Mechanics*, Vol. 54, No. 2, 1987, pp. 258 – 262.
- [17] Hodges, D. H., *Nonlinear composite beam theory*, AIAA, Washington, D.C., 2006.
- [18] Berdichevsky, V. L., “Variational-asymptotic method of constructing a theory of shells,” *PMM*, Vol. 43, No. 4, 1979, pp. 664 – 687.
- [19] Roy, S. and Yu, W., “A Variational-Asymptotic Theory of Smart Slender Structures,” *Proceedings of the 2005 ASME International Mechanical Engineering Congress and Exposition*, ASME, Orlando, Florida, Nov. 5–11 2005.
- [20] Bauchau, O. A. and Kang, N. K., “A Multibody Formulation for Helicopter Structural Dynamic Analysis,” *Journal of the American Helicopter Society*, Vol. 38, No. 2, 1993, pp. 3 – 14.
- [21] Bauchau, O. A. and Theron, N. J., “Energy Decaying Schemes for Nonlinear Beam Models,” *Computer Methods in Applied Mechanics and Engineering*, Vol. 134, No. 1-2, 1996, pp. 37 – 56.
- [22] Palacios, R., *Asymptotic Models of Integrally-Strained Slender Structures for High-Fidelity Nonlinear Aeroelastic Analysis*, Ph.D. thesis, Aerospace Engineering, University of Michigan, 2005.
- [23] Palacios, R. and Cesnik, C. E. S., “Cross-sectional analysis of nonhomogeneous anisotropic active slender structures,” *AIAA Journal*, Vol. 43, No. 12, 2005, pp. 2624–2638.
- [24] Robbins, D. H. and Reddy, J. N., “Analysis of piezoelectrically actuated beams using a layerwise displacement theory,” *Computers & Structures*, Vol. 41, No. 2, 1991, pp. 265 – 279.
- [25] Saravanos, D. and Heyliger, P. R., “Coupled layerwise analysis of composite beams with embedded piezoelectric sensors and actuators,” *Journal of Intelligent Material Systems and Structures*, Vol. 6, No. 3, 1995, pp. 350 – 363.
- [26] Krommer, M. and Irschik, H., “On the influence of the electric field on free transverse vibrations of smart beams,” *Smart Materials and Structures*, Vol. 8, No. 3, 1999, pp. 401 – 410.